Available online at www.sciencedirect.com
ScienceDirect
Trans. Nonferrous Met. Soc. China 35(2025) 3933−3948
Transactions of Nonferrous Metals Society of China
www.tnmsc.cn

Loss behavior of Ni and Co during Al and Sc enrichment from HNO_3 leach liquor of saprolitic laterite ore

Jian-cheng YU[1,2], Bao-zhong MA[1,2], Long-fei SHI[1,2], Zhi-he CAO[1,2], Yu-bo LIU[1,2], Cheng-yan WANG[1,2]

1. State Key Laboratory of Advanced Metallurgy, University of Science and Technology Beijing, Beijing 100083, China;
2. School of Metallurgical and Ecological Engineering, University of Science and Technology Beijing, Beijing 100083, China

Received 25 April 2024; accepted 18 November 2024

Abstract: The loss pathways of Ni and Co during Al and Sc enrichment were analyzed in the HNO_3 leach liquor of saprolitic laterite ore. Although over 99% of Al and Sc can be enriched, about 40% of Ni and Co are also lost. The adsorption of Al−Sc precipitate is an important cause of Ni and Co loss. Subsequently, the precipitation behavior of metal ions in the different nitrate solutions was studied. The results confirm that Ni^{2+} and Co^{2+} do not hydrolyze to form their respective hydroxides. Ni^{2+}, Co^{2+} and Mg^{2+} can form composite hydroxides with precipitated $Al(OH)_3$, decreasing the pH at which Ni^{2+} and Co^{2+} begin to precipitate, causing their co-precipitation loss. A high Mg^{2+} concentration enhances the formation of these composite hydroxides. Finally, titration curves for different nitrate systems were determined, further demonstrating the formation of Me−Al composite hydroxides and revealing a formation trend of Mg−Al > Co−Al > Ni−Al.

Key words: laterite ore; HNO_3 leach liquor; metal loss; hydrolysis precipitation; composite hydroxide

1 Introduction

With the sulfide nickel ore drying up gradually, the development of laterite ore has attracted increasing attention. The contribution of laterite ore to global Ni production has increased from less than 10% in 1950 to over 70% at present [1]. Laterite ore is a complex strategic mineral resource rich in Ni, Co, Mg, Al, and so on. Importantly, Sc is also found within laterite ore [2]. Sc is an important strategic metal and raw material for manufacturing special alloys [3]. The discovery of Sc-rich laterite ore indicates that this type of ore is an important potential source for extracting Sc. Generally, laterite ore can be divided into limonitic, transitional, and saprolitic types [4]. The saprolitic laterite ore has the characteristics of high Si, Mg and Ni content, and low Fe content, and is mainly composed of serpentinite, magnetite, and goethite [5]. However, limonitic laterite ore has high Fe content and low Si, Mg, and Ni content, mainly composed of goethite, hematite, and silica [6,7]. The content and composition of transitional laterite ore are between those of limonitic and saprolitic laterite ores.

For the treatment of saprolitic laterite ore, pyrometallurgy is usually applied [8]. The typical process involves rotary kiln pre-reduction and electric furnace melting to produce Ni−Fe alloys (RKEF) [9]. This process is easy to operate and has

Corresponding author: Bao-zhong MA, Tel: +86-18601365281, E-mail: bzhma_ustb@yeah.net;
Cheng-yan WANG, Tel: +86-13651380586, E-mail: chywang@yeah.net
https://doi.org/10.1016/S1003-6326(25)66922-6

a high Ni recovery yield. However, the high smelting temperature (1300−1600 °C) leads to high electricity consumption. More importantly, the RKEF process only focuses on recovering Ni while ignoring Mg, Co and Sc in saprolitic laterite ore [10]. Generally speaking, the saprolitic laterite ore contains up to 20%−30% MgO [11,12], and the potential of Mg may even exceed that of Ni. The potential of Co and Sc cannot be ignored either. In the hydrometallurgical routes, H_2SO_4 leaching has been applied to simultaneously extracting Ni and Co [13−15]. The advantages of H_2SO_4 leaching include a mature process and easily controllable operating conditions. Nevertheless, this method has significant drawbacks. It suffers from low resource utilization efficiency because the S-bearing leach residue that is difficult to utilize is produced and the treatment of $MgSO_4$ solution after precipitation also poses a huge challenge [16,17]. Additionally, high reagent consumption is inevitable, as both leaching agents and neutralizing agents cannot be effectively regenerated.

Addressing the aforementioned shortcomings, our research team innovatively proposed the HNO_3 leaching technology to treat saprolitic laterite ore. The main steps are as follows: (1) HNO_3 leaching to extract Ni, Co, Mg and Sc; (2) Stepwise precipitation to obtain Al−Sc precipitate and Ni−Co precipitate by using MgO; (3) The $Mg(NO_3)_2$ solution is concentrated and pyrolyzed to regenerate HNO_3 and produce MgO. This process has high resource utilization efficiency and realizes the comprehensive utilization of Ni, Co, Mg, and Sc. In addition, the $Mg(NO_3)_2$ pyrolysis enables the circular regeneration of the leaching agent (HNO_3) and the neutralizing agent (MgO), resulting in reduced reagent consumption. In the leachate, relying on the different precipitation pHs of metal ions, MgO is used as a neutralizing agent to gradually separate and enrich valuable metals [18,19]. Due to their lower precipitation pH compared with Ni, Co and Mg, Al and Sc tend to precipitate together to form Al−Sc precipitate [20]. Theoretically, since the precipitation pH of Ni, Co and Mg is higher than that of Al and Sc, they do not precipitate during Al and Sc enrichment. However, in practical applications, it is found that a portion of Ni, Co and Mg always precipitate together with Al and Sc resulting in their loss [21,22]. Importantly, the loss behavior and mechanism of Ni and Co in this process are not clear.

Current research on the separation and enrichment of valuable metals in HNO_3 medium is limited, primarily focusing on optimizing precipitation process parameters, while minimally exploring precipitation behavior and metal ion interaction mechanisms. To enhance the recovery efficiency of Ni and Co while minimizing their loss, elucidating the precipitation behavior of Ni and Co during the Al and Sc neutralization process is crucial. This work systematically investigated the loss pathways of Ni and Co during Al and Sc enrichment, innovatively elucidating their precipitation behavior and loss mechanisms. Furthermore, it reveals the rules and trends of metal ion interactions during hydrolysis precipitation. Firstly, the influence of temperature and pH on the precipitation efficiency of Al, Sc, Ni and Co was investigated in the process of MgO neutralization precipitation. Then, the precipitation behavior of Al and Sc and loss pathways of Ni and Co were analyzed by studying the precipitation characteristics of corresponding metal ions in single-component and mixed nitrate solutions. Finally, the titration curves of different nitrate systems were studied, confirming the specific loss mechanism of Ni and Co and revealing the interaction trend between metal ions. This work provides theoretical support for the efficient separation of valuable metals from complex laterite ore acid leachate, thereby laying a solid foundation for improving the utilization efficiency of laterite ore resources.

2 Experimental

2.1 Materials and reagents

The used leach liquor comes from the HNO_3 leaching process of saprolitic laterite ore and has the following main chemical composition: 3.71 g/L Ni, 78×10^{-3} g/L Co, 0.079 g/L Fe, 5.63 g/L Al, 7.5×10^{-3} g/L Sc, and 45.15 g/L Mg. Due to the high Mg content in saprolitic laterite ore, the Mg concentration in leach liquor is as high as 45.15 g/L. Additionally, selective removal of Fe was carried out after leaching, which results in a low concentration of Fe. Other reagents used include HNO_3 (65 wt.%), $Al(NO_3)_3\cdot9H_2O$, Sc_2O_3, $Ni(NO_3)_2\cdot$

$6H_2O$, $Co(NO_3)_2·6H_2O$, and $Mg(NO_3)_2·6H_2O$. The MgO utilized originates from the pyrolysis process of $Mg(NO_3)_2·6H_2O$, which has been confirmed in our previous research [23], and the purity of prepared MgO product is 98.29%.

2.2 Experimental procedure

In a typical experimental process, 100 mL of leachate was placed in a water bath, and a digital pH detector was inserted to monitor the pH in real-time. An appropriate amount of water was mixed with MgO powder to prepare a MgO slurry of 200 g/L. The MgO slurry was slowly added until the solution pH reached the predetermined value. After stirring and reacting for 1 h, the solution was filtered to separate the wet Al−Sc precipitate from the leachate. Subsequently, the wet Al−Sc precipitate was washed repeatedly with deionized water, with each washing step conducted at a temperature of 25 °C for 3 h. The volumes and ion concentrations of the leachate and washing solutions were measured. The Al/Sc precipitation rate and the Ni/Co loss rate (η) were calculated using Eq. (1), while the Ni/Co adsorption rate (μ) was calculated using Eq. (2) (V_0, V_1 and V_2 represent the volumes of the original solution, leachate and washing solution, respectively; C_0^i, C_1^i and C_2^i represent the concentrations of component i in the original solution, leachate, and washing solution, respectively).

$$\eta = \left(1 - \frac{V_1 C_1^i}{V_0 C_0^i}\right) \times 100\% \quad (1)$$

$$\mu = \frac{V_2 C_2^i}{V_0 C_0^i} \times 100\% \quad (2)$$

On this basis, the precipitation behaviors of Al^{3+}, Sc^{3+}, Ni^{2+} and Co^{2+} were further investigated during MgO neutralization precipitation. A $Sc(NO_3)_3$ solution was prepared by dissolving Sc_2O_3 in HNO_3, while other nitrate solutions were directly prepared by dissolving the respective nitrate salts in deionized water. Finally, the titration curves of single-component and mixed nitrate solutions were measured. During this process, a 0.5 mol/L $Al(NO_3)_3$ solution was prepared, and $Ni(NO_3)_2$, $Co(NO_3)_2$, and $Mg(NO_3)_2$ were each prepared as 0.025 mol/L solutions. The mixed nitrate solutions were prepared in a molar ratio of Al^{3+} to Me^{2+} as 2:1 (where Me^{2+} represents Ni^{2+}, Co^{2+}, or Mg^{2+}). The titration process involves adding alkali or acid to the nitrate solution via a constant-flow pump. The forward titration process involves adding 1.5 mol/L of KOH to a 100 mL mixed nitrate system at a drop speed of 0.4 mL/min. The reverse titration process involves adding 1.0 mol/L of HNO_3 to the solution at a drop speed of 0.4 mL/min. The variation curves of KOH and HNO_3 addition volumes versus solution pH were recorded.

2.3 Analytical methods

The metal ion concentrations in the solution were detected using inductively coupled plasma–optical emission spectroscopy (ICP–OES, Optima 7000DV, PerkinElmer). X-ray diffraction (XRD, D5000, Siemens) was applied to analyzing the phase composition of the obtained precipitate. In addition, scanning electron microscopy (SEM, JSM−7001 F), coupled with an energy dispersive spectrometer (EDS, GENESIS), was used to analyze the morphology and elemental distribution of the hydrolysis precipitates under varying conditions.

3 Results and discussion

3.1 Precipitation efficiency of Al and Sc and potential loss routes of Ni and Co

A detailed investigation was conducted on the precipitation behavior of valuable metals. In Fig. 1(a), the Al and Sc precipitation rates gradually increase with the rising pH at 50 °C. Moreover, the changes in Al and Sc precipitation curves are consistent, demonstrating that their precipitation behaviors are similar. At pH=4.5, 99.32% of Al and 99.18% of Sc are precipitated. From the change curves of Ni and Co loss, the loss rates of Ni and Co also gradually increase as the pH rises, reaching 43.2% and 40.3%, respectively at pH 4.5. Furthermore, the effects of hydrolysis temperature are studied at pH 4.5, as presented in Fig. 1(b). Overall, temperature changes have a relatively low impact on precipitation efficiency compared with pH. As the temperature rises from 25 to 50 °C, the precipitation rate of Al increases from 94.69% to

99.32%, and the precipitation rate of Sc increases from 92.18% to 99.18%. As the temperature is above 50 °C, the loss rates of Ni and Co also show a slight increasing trend. The loss rate of Ni exceeds 40% and that of Co exceeds 37% while the temperature exceeds 40 °C. The above results indicate that although over 99% of Al and Sc can be efficiently enriched during neutralization precipitation, about 40% of Ni and Co are also lost. Moreover, a small amount of Fe^{3+} in the solution is also completely precipitated during this process.

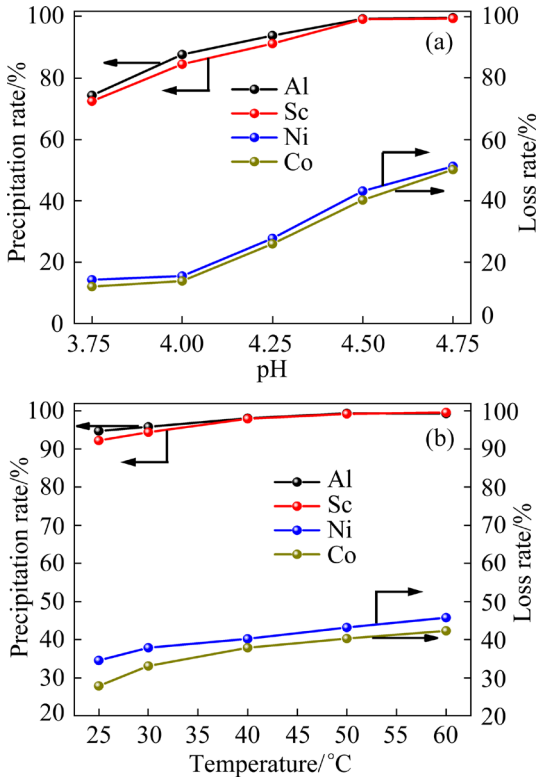

Fig. 1 Effects of pH (a) and temperature (b) on precipitation of Al and Sc and loss of Ni and Co

Undoubtedly, to reduce the loss of Ni and Co during Al and Sc enrichment, it is necessary to first clarify their possible loss pathways. Presently, laterite ore is usually leached with H_2SO_4 [24]. After leaching, Fe^{3+} and Al^{3+} are removed together by adjusting the solution pH with CaO or $CaCO_3$, and some Ni and Co are also inevitably lost in this process [25,26]. Based on the hydrolysis and interaction laws of metal ions, it can be inferred that the loss behavior of Ni and Co in the HNO_3 medium may include the following three pathways: (1) The Al−Sc precipitate generated during the hydrolysis process can adsorb Ni^{2+} and Co^{2+}; (2) $Mg(OH)_2$ with high alkalinity and low solubility is formed after hydration of MgO, which leads to high alkalinity in some areas of the liquid phase, even exceeding the pH at which Ni^{2+} and Co^{2+} begin to hydrolyze. Thus, Ni^{2+} and Co^{2+} hydrolyze into their respective hydroxides; (3) Ni and Co form composite hydroxides with Al, leading to their co-precipitation loss. A schematic diagram of the three possible loss pathways is shown in Fig. 2.

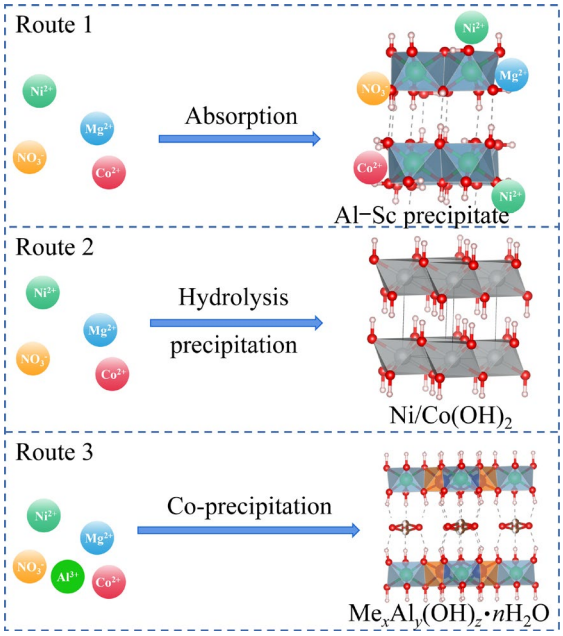

Fig. 2 Schematic diagram of possible loss routes for Ni and Co

3.2 Adsorption loss of Ni and Co

To investigate the adsorption degree of Al−Sc precipitate on Ni^{2+} and Co^{2+}, the precipitate underwent multiple consecutive washings. The wash solution from the last three washes contained negligible concentrations of Ni^{2+} and Co^{2+}, indicating that Ni^{2+} and Co^{2+} were thoroughly washed away. Subsequently, the total amount of Ni^{2+} and Co^{2+} in the wash solutions was calculated and taken as a measure of the total adsorbed quantity of Al−Sc precipitate. The specific results are presented in Fig. 3. According to Fig. 3(a), under the fixed conditions of 50 °C, the adsorption rates of both Ni and Co gradually increase with rising pH, attributable to the increased amount of Al−Sc precipitate generated. At pH=4.5, the adsorption rates of Ni and Co reach 9.35% and 12.50%, respectively. Temperature also has a certain

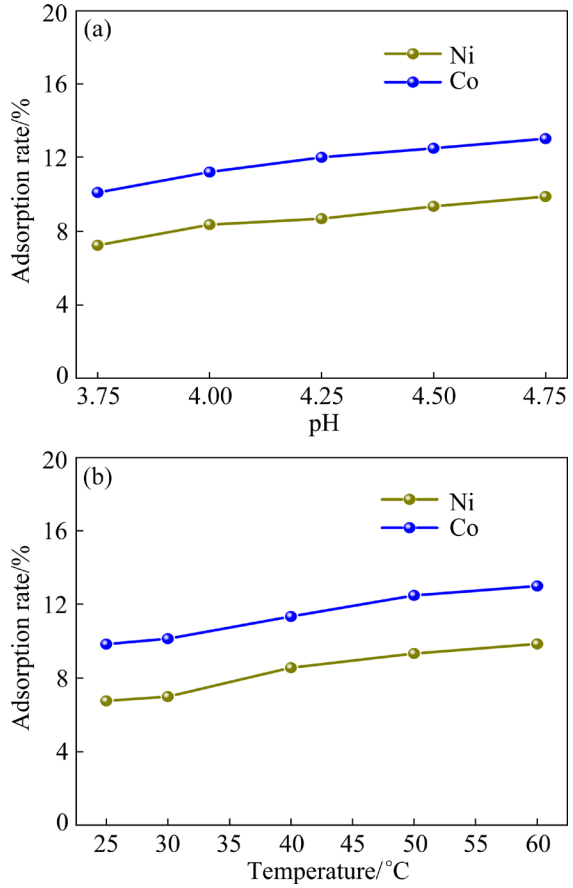

Fig. 3 Effects of pH (a) and temperature (b) on absorption loss of Ni and Co

effect on the adsorption rates of Ni and Co at pH 4.5, as displayed in Fig. 3(b). As the temperature rises from 25 to 50 °C, the Ni adsorption rate increases from 6.78% to 9.35%, and the Co adsorption rate increases from 9.86% to 12.50%. Increasing the temperature to 60 °C further improves the adsorption rates of Ni and Co to 9.87% and 13.01%, respectively. High temperature accelerates the thermal motion of ions and improves the collision frequency between the Al−Sc precipitate and metal ions, thereby enhancing their adsorption efficiency. Furthermore, it is worth noting that the Co adsorption rate tends to be slightly higher than that of Ni under the same conditions. This is because $Co(OH)_2$ has a slightly stronger alkalinity than $Ni(OH)_2$, and thus Co^{2+} is more easily adsorbed [27]. Based on the aforementioned results, it can be concluded that the adsorption of Al−Sc precipitate (Route 1 in Fig. 2) is one of the important pathways for the loss of Ni and Co.

3.3 Hydrolysis of Ni and Co into their hydroxides

After the MgO powder is prepared into a slurry and added to the solution, it undergoes the hydration reaction to form $Mg(OH)_2$ on the particle surface. Due to the relatively low solubility and high alkalinity of $Mg(OH)_2$ (saturated pH of about 10.0) [28], the alkalinity of the hydrated particle surface is high, even exceeding the pH at which Ni^{2+} and Co^{2+} begin to hydrolyze. Ni^{2+} and Co^{2+} may hydrolyze to form $Ni(OH)_2$ and $Co(OH)_2$, respectively, as precipitates. To verify this possibility, the precipitation behavior of Ni^{2+} and Co^{2+} were studied in the single-component $Ni(NO_3)_2$ and $Co(NO_3)_2$ solutions, respectively. From Fig. 4(a), the pH range for the onset to completion of Ni^{2+} precipitation is 7.10−9.10, which closely matches the theoretical precipitation pH range. Similarly, in Fig. 4(b), the pH range for the onset and completion of Co^{2+} precipitation is 7.50−9.20, which also agrees with the theoretical range.

The precipitation behavior of Ni^{2+} and Co^{2+} confirms that they do not undergo premature precipitation in the single-component $Ni(NO_3)_2$ and $Co(NO_3)_2$ solutions, and they start precipitating only as the solution pH reaches the theoretical hydrolysis pH. However, the solution pH during Al and Sc enrichment is much lower than the theoretical pH at which Ni^{2+} and Co^{2+} begin to precipitate. In addition, given the high Mg concentration in leach liquor, $Mg(NO_3)_2$ (with a Mg^{2+} concentration of 45 g/L) was added to prepare mixed nitrate solution, specifically $Ni(NO_3)_2$ with $Mg(NO_3)_2$ and $Co(NO_3)_2$ with $Mg(NO_3)_2$, respectively. As shown in Figs. 4(c) and (d), the pH ranges of Ni^{2+} and Co^{2+} precipitation are 7.22−8.89 and 7.42−9.03, respectively. Compared with the pH ranges observed in Figs. 4(a) and (b), the pH ranges for Ni^{2+} and Co^{2+} precipitation in the mixed solutions have hardly changed significantly, suggesting that their hydrolysis process is largely unaffected by the presence of high Mg^{2+} concentration.

As demonstrated above, Ni^{2+} and Co^{2+} do not undergo premature precipitation; they only begin to precipitate when the solution pH rises to a level close to their theoretical precipitation points. However, during the enrichment of Al and Sc with MgO slurry, the solution pH consistently remains

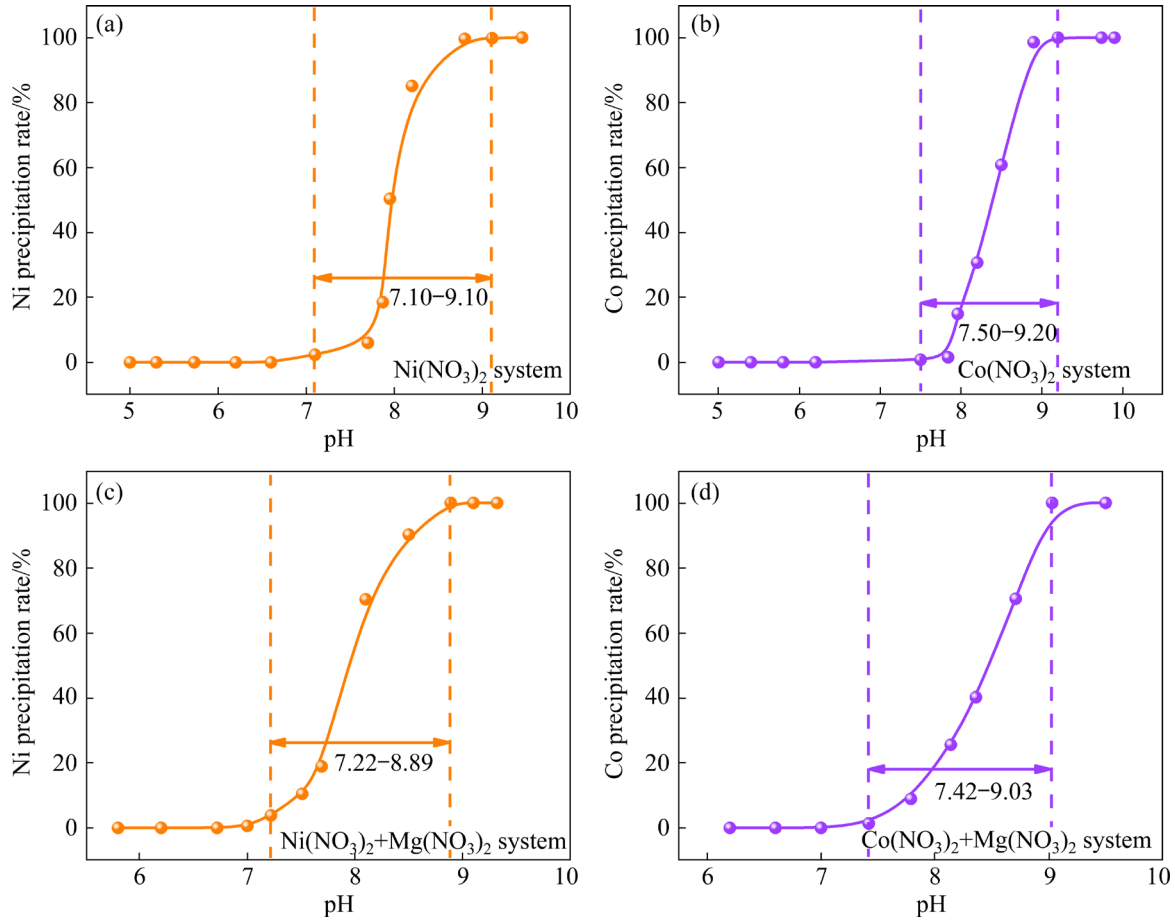

Fig. 4 pH ranges of Ni and Co precipitation in different nitrate systems

below the threshold, where Ni^{2+} and Co^{2+} begin to precipitate. Thus, despite the possibility of localized areas with high alkalinity emerging in the liquid phase, Route 2 (Fig. 2) that is the hydrolysis of Ni^{2+} and Co^{2+} into their respective hydroxide precipitates, is not the primary reason for their loss.

3.4 Co-precipitation of multiple metals to form composite hydroxide

3.4.1 Precipitation behavior of Al and Sc

Research [26] has shown that Ni^{2+} and Co^{2+} can form complex compounds with Fe^{3+} or Al^{3+} in the process of removing Fe and Al from the H_2SO_4 leaching solution. Similarly, in this system, Ni^{2+} and Co^{2+} may also form complex compounds with Al^{3+}, causing their co-precipitation loss. To further reveal the loss behavior of Ni and Co during Al and Sc enrichment and determine the phase composition of the Al−Sc precipitate, the precipitation behaviors of Al and Sc were first studied in single-component nitrate solutions. As shown in Figs. 5(a) and (b), the pH ranges for Al^{3+} and Sc^{3+} from beginning to complete precipitation are 3.49−6.20 and 3.47−6.57, respectively.

Furthermore, this study focuses on saprolitic laterite ore with high Mg content, to further clarify the effect of high Mg concentration on Al^{3+} and Sc^{3+} hydrolysis. Two separate mixed nitrate systems were designed: one containing $Al(NO_3)_3$ and $Mg(NO_3)_2$, and another containing $Al(NO_3)_3$, $Sc(NO_3)_3$ and $Mg(NO_3)_2$. The Al and Sc precipitation behavior as a function of pH is shown in Figs. 5(c) and (d). In Fig. 5(c), the pH range for Al^{3+} hydrolysis precipitation is 2.66−4.91. Compared to Fig. 5(a), the pH range of Al^{3+} precipitation drops to varying degrees. This is because the high Mg concentration can inhibit the dissolution and release of OH^- from $Mg(OH)_2$. As expressed in Eq. (3), a high Mg concentration promotes the reverse reaction, reducing the solubility of $Mg(OH)_2$. This, in turn, exacerbates local alkaline regions in the liquid phase, leading to the premature precipitation of Al^{3+}. Similarly, in the mixed system of Fig. 5(d), the precipitation pH ranges of Al^{3+} and Sc^{3+} are

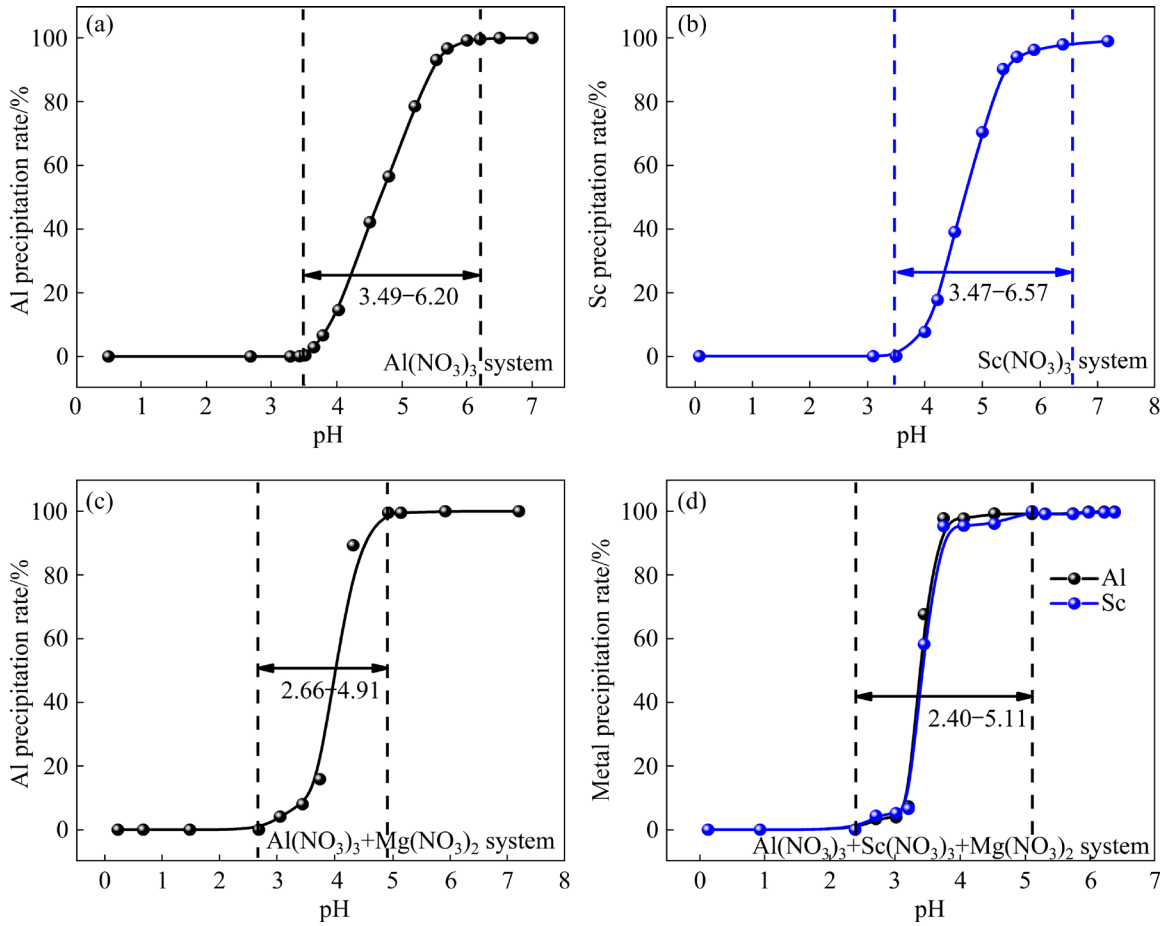

Fig. 5 pH ranges of Al and Sc precipitation in different nitrate systems

extremely close, and their range is 2.40−5.11, which is significantly lower than that of the single-component $Al(NO_3)_3$ and $Sc(NO_3)_2$ solution. Thus, the high Mg concentration leads to a reduction in the pH range within which Al^{3+} and Sc^{3+} precipitate.

$$MgO+H_2O=Mg(OH)_2\rightleftharpoons Mg^{2+}+2OH^- \quad (3)$$

XRD characterization was further performed on the precipitate in Fig. 6. The precipitate formed is non-crystalline in the single-component $Al(NO_3)_3$ and $Sc(NO_3)_3$ solution. In contrast, the precipitate consists of $Al(OH)_3$ and $MgAl_2(OH)_8$ in the mixed $Al(NO_3)_3$ and $Mg(NO_3)_2$ solution, demonstrating that Al^{3+} not only hydrolyzes to form $Al(OH)_3$ but also reacts with Mg^{2+} to form Mg−Al composite hydroxides. Furthermore, $Al(OH)_3$ and $MgAl_2(OH)_8$ can also be observed in the mixed nitrate solution of $Al(NO_3)_3$, $Mg(NO_3)_2$, and $Sc(NO_3)_3$, and the diffraction peak intensity of $MgAl_2(OH)_8$ is enhanced, indicating that the high Mg concentrations can further promote the formation of $MgAl_2(OH)_8$.

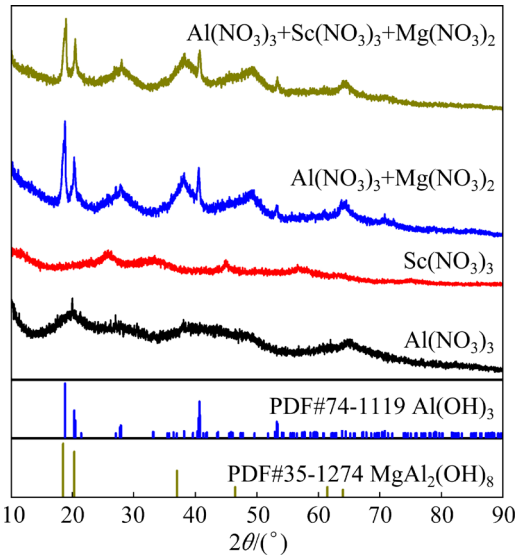

Fig. 6 XRD patterns of obtained precipitates from different nitrate solutions

Although the precipitate obtained from single-component $Al(NO_3)_3$ solutions is amorphous, the SEM−EDS analysis thereof shows interesting

phenomena. In Fig. 7(a), only Al and O are detected, and this is attributed to $Al(OH)_3$ generated by Al^{3+} hydrolysis. However, in Fig. 7(b), a region where Al, O and Mg coexistence can be observed, which is strong evidence for the formation of Mg−Al composite hydroxides. Perhaps due to the poor crystallization, the corresponding diffraction peaks are absent in the XRD pattern. The presence of Mg is primarily attributed to the utilization of MgO as a neutralizing agent in this study. The SEM−EDS analysis was also performed on the obtained precipitate of the mixed nitrate solution. As indicated by Figs. 8(a) and (b), Sc also enters the precipitate, with regions enriched in Al, O and Sc, as well as regions enriched in Al, O, Mg and Sc, observable. The reason is that Al^{3+} and Sc^{3+} share similar ionic radii and valences, allowing Sc^{3+} to potentially replace Al^{3+} in $Al(OH)_3$ or $MgAl_2(OH)_8$. Therefore, Sc can also be detected in the Al-enriched region. Overall, Sc^{3+} has a low concentration and ion strength, exerting a minimal on the hydrolysis process.

As indicated above, it can be concluded that Al^{3+} not only hydrolyzes to form $Al(OH)_3$ but also interacts with Mg^{2+} to form $MgAl_2(OH)_8$ during MgO neutralization precipitation. Compared to a single-component $Al(NO_3)_3$ solution, the weak diffraction peak of $Al(OH)_3$ can be observed in the precipitate obtained from the mixed $Al(NO_3)_3$ and $Mg(NO_3)_2$ solution. This is primarily due to the high ionic concentrations, which lead to significant ionic strength and consequently reduce the activity coefficient of Al^{3+} in mixed nitrate solutions. This, in turn, slows down the hydrolysis rate of Al^{3+}, favoring the precipitation and growth of larger particles, and promoting the transformation of some $Al(OH)_3$ colloids into crystalline states. Furthermore, a high Mg^{2+} concentration not only promotes the formation of $MgAl_2(OH)_8$ but also causes a decline in the pH at which Al^{3+} initiates precipitation. Generally speaking, $MgAl_2(OH)_8$ is formed under alkaline conditions [29]. However, in this study, despite the real-time monitoring of the solution pH, which never exceeded 7.0, $MgAl_2(OH)_8$ was still generated. Because the MgO particles hydrate to form $Mg(OH)_2$ with low solubility and high alkalinity, resulting in some localized high alkaline regions in the liquid phase, and thus providing conditions for the formation of $MgAl_2(OH)_8$.

3.4.2 Precipitation behavior of Ni and Co

To further clarify the precipitation behavior of Ni and Co, different mixed nitrate solutions containing $Ni(NO_3)_2$ or $Co(NO_3)_2$ were designed. In

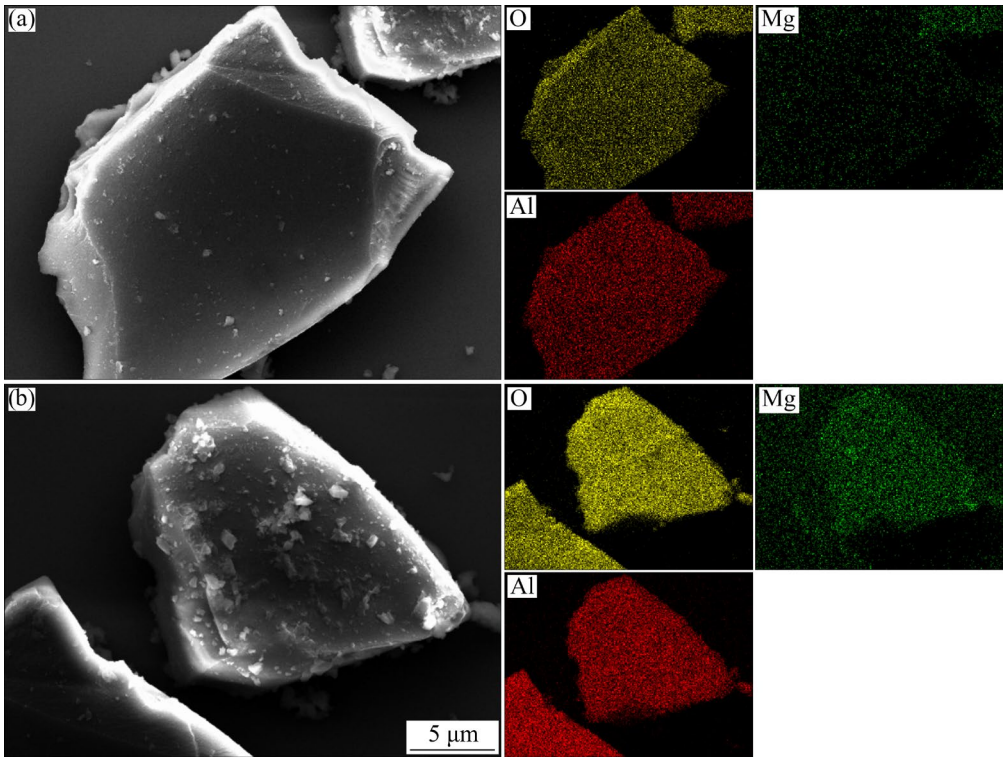

Fig. 7 SEM−EDS analysis of precipitated aluminum hydroxide (a) and composite hydroxide (b) in $Al(NO_3)_3$ solution

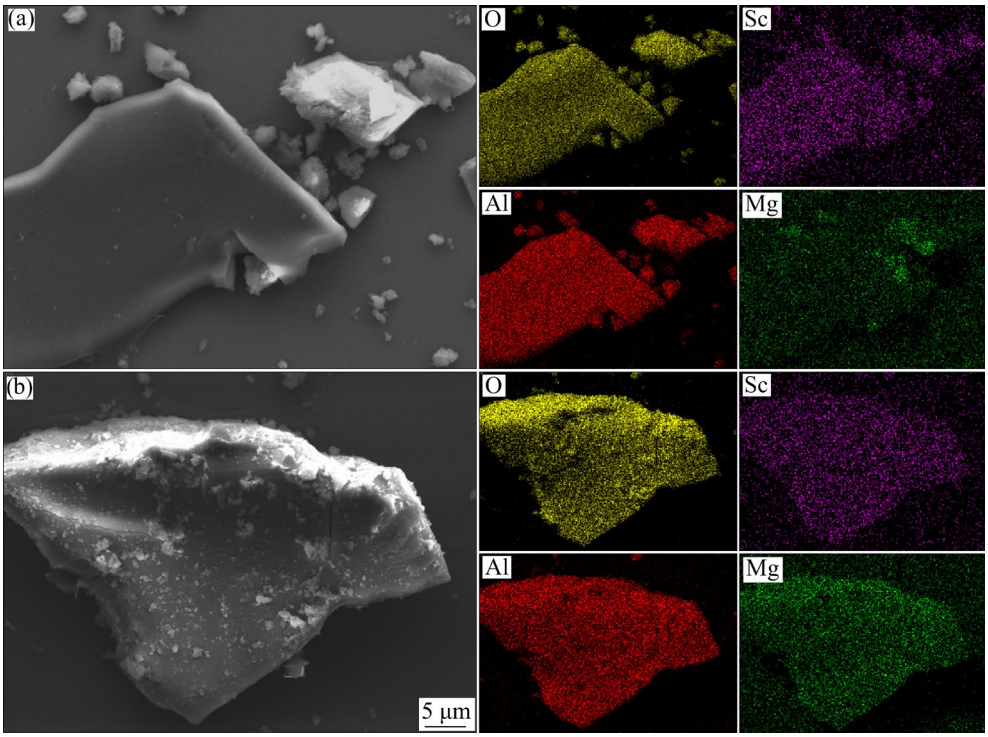

Fig. 8 SEM−EDS analysis of precipitated aluminum hydroxide (a) and composite hydroxide (b) in mixed $Al(NO_3)_3$, $Sc(NO_3)_3$ and $Mg(NO_3)_2$ solution

the real HNO_3 leaching solution, the Sc^{3+} concentration is low, and its hydrolysis process has little effect on Ni and Co. Therefore, in this study, the effects of Al^{3+} and Mg^{2+} are mainly investigated. Firstly, the Ni precipitation rate in the mixed $Al(NO_3)_3$ and $Ni(NO_3)_2$ solution is studied as a function of pH (Fig. 9(a)). The precipitation pH range of Al^{3+} (3.26−6.04) is similar to that in a single-component $Al(NO_3)_3$ solution. Generally, the pH at which Ni^{2+} begins to precipitate is around 7.5 in the single-component $Ni(NO_3)_2$ solution, but its precipitation pH range significantly drops to 3.26−7.06 in the mixed solution. Furthermore, as shown in Fig. 9(b), in the mixed solution of $Al(NO_3)_3$, $Ni(NO_3)_2$ and $Mg(NO_3)_2$ (Mg^{2+} concentration of 45 g/L), the precipitation pH ranges for Al^{3+} and Ni^{2+} decline to 2.65−4.50 and 2.95−6.82, respectively. The presence of high Mg^{2+} concentration in the solution likely affects the availability of OH^-, inhibiting its release and promoting the interaction between Al^{3+} and Mg^{2+} to form Mg−Al composite hydroxides, thereby lowering the pH at which Al^{3+} begins to precipitate. On the other hand, Mg^{2+} has a relatively weak impact on the Ni precipitation process in the single-component $Ni(NO_3)_2$ solution (Fig. 4(c)). On the basis of the results, it can be concluded that the drop in the pH range where Ni^{2+} precipitates is closely related to the Al^{3+} hydrolysis.

Similarly, the Co^{2+} precipitation behavior is similar to that of Ni^{2+}. In the mixed $Al(NO_3)_3$ and $Co(NO_3)_2$ solution (Fig. 9(c)), the pH range for Co^{2+} precipitation is 3.16−7.28. Compared with the results from a single-component $Co(NO_3)_2$ solution in Fig. 4(b), the pH at which Co^{2+} begins to precipitate also significantly decreases. In the mixed solution of $Al(NO_3)_3$, $Co(NO_3)_2$, and $Mg(NO_3)_2$ (Mg^{2+} concentration of 45 g/L) (Fig. 9(d)), the Co^{2+} precipitation pH drops to 2.99−6.87. Moreover, a high Mg^{2+} concentration also has a relatively minor impact on the Co^{2+} precipitation process. Hence, the decrease in the pH range of Co^{2+} precipitation is also closely related to the Al^{3+} precipitation.

Figure 10 shows the XRD patterns of the obtained precipitate from different nitrate solutions. In the mixed $Al(NO_3)_3$ and $Ni(NO_3)_2$ solution, the phase composition of the precipitate includes $Al(OH)_3$, $Mg(OH)_2$ and $Mg_4Al_2(OH)_{14}·3H_2O$. The presence of the generated $Al(OH)_3$ colloid enveloping the surface of hydrated $Mg(OH)_2$ prevents its further dissolution, allowing the diffraction peak of $Mg(OH)_2$ to be detected. The existence of $Mg_4Al_2(OH)_{14}·3H_2O$ confirms the

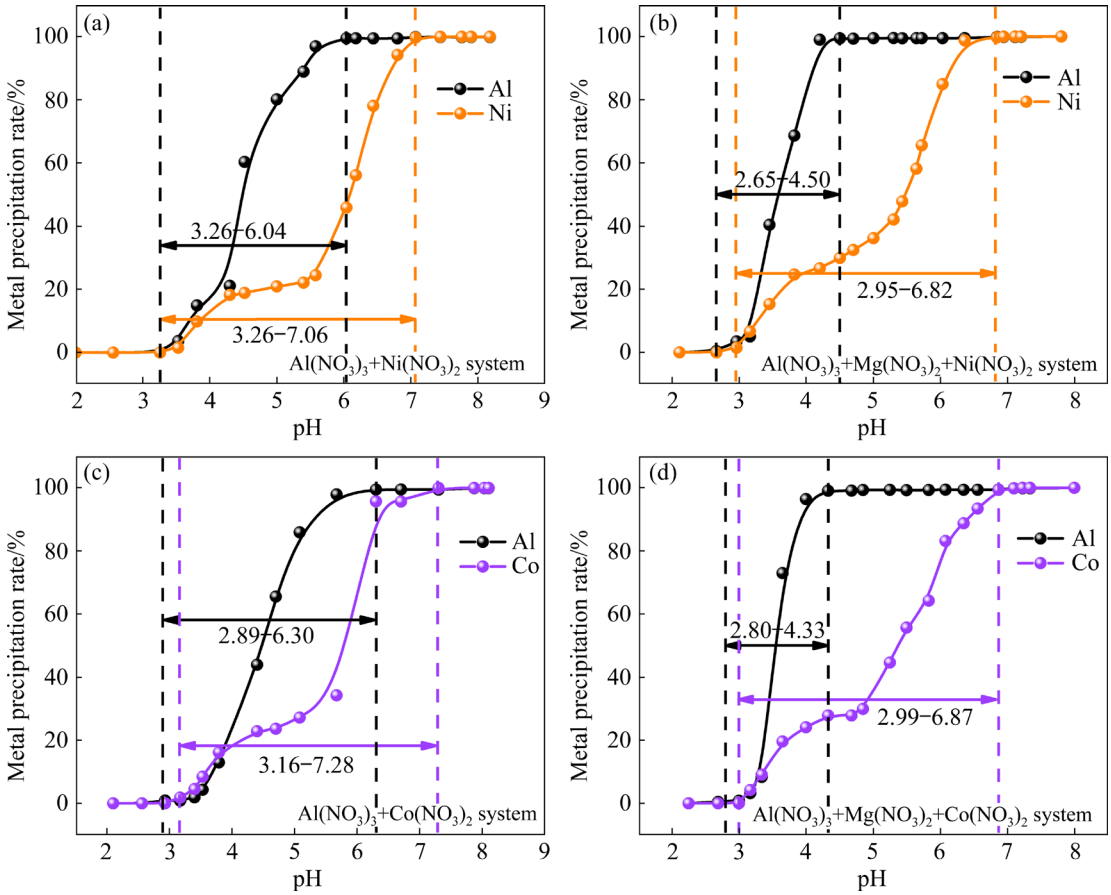

Fig. 9 pH ranges of Al, Ni and Co precipitation in different nitrate systems

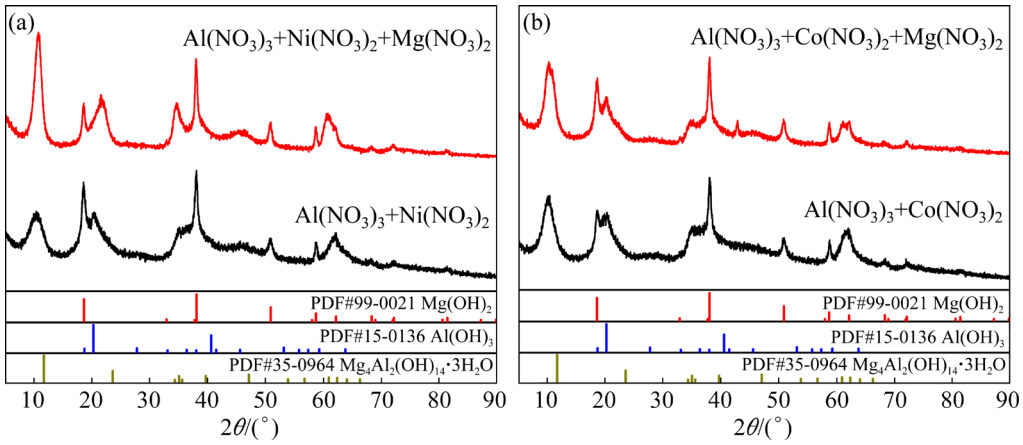

Fig. 10 XRD patterns of obtained precipitates for different nitrate solutions

reaction between Mg^{2+} and Al^{3+} to form Mg−Al composite hydroxides. Furthermore, the chemical formula of the Mg−Al composite hydroxide obtained in the mixed $Al(NO_3)_3$ and $Ni(NO_3)_2$ solution differs from that in the mixed $Al(NO_3)_3$ and $Mg(NO_3)_2$ solution, due to differences in the Mg and Al ratio and pH between the two systems [30]. Notably, despite the absence of notable differences in the phase composition of the precipitates formed in the ternary nitrate solution (consisting of $Al(NO_3)_3$, $Ni(NO_3)_2$, and $Mg(NO_3)_2$) as compared to the binary solution of $Al(NO_3)_3$ and $Ni(NO_3)_2$, there is a marked enhancement in the diffraction peak intensity of $Mg_4Al_2(OH)_{14}·3H_2O$. This suggests that a high Mg concentration can further promote the formation of $Mg_4Al_2(OH)_{14}·3H_2O$. As

shown in Fig. 10(b), the diffraction peaks of $Al(OH)_3$, $Mg(OH)_2$ and $Mg_4Al_2(OH)_{14}·3H_2O$ can also be observed in the obtained precipitate from the mixed $Al(NO_3)_3$ and $Co(NO_3)_2$ solution, as well as the mixed solution of $Al(NO_3)_3$, $Co(NO_3)_2$ and $Mg(NO_3)_2$.

No phase composition containing Ni and Co was found in the XRD patterns of the precipitates. Further analysis of the precipitates was carried out through the SEM−EDS characterization. The precipitate obtained from the mixed solution of $Al(NO_3)_3$, $Ni(NO_3)_2$ and $Mg(NO_3)_2$ (Fig. 11(a)) consists of irregular blocks. The elements O, Al and Mg are uniformly distributed within the red outline, without any trace of Ni. This part of the precipitate is the Mg−Al composite hydroxide formed by Mg^{2+} and Al^{3+}. In some regions, it is found that O, Al, Mg and Ni are evenly distributed, indicating that Ni^{2+} does not hydrolyze to produce $Ni(OH)_2$. Instead, it forms composite hydroxides with Mg^{2+} and Al^{3+}. During the formation of composite hydroxides, Mg^{2+} replaces Al^{3+} in the Al−O octahedral structure of $Al(OH)_3$, and at the same time, Ni^{2+} can also enter it to replace Al^{3+} to form Mg−Ni−Al composite hydroxides ($Mg_xNi_{1-x}Al_y(OH)_z·nH_2O$) [31]. The replacement of Ni^{2+} does not change the crystal structure of the Mg−Al composite hydroxides, and therefore no Ni-containing phases are observed in the XRD pattern. Co^{2+} demonstrates similar precipitation behavior to Ni^{2+}. Figure 11(b) shows regions where O, Al, and Mg coexist, as well as regions where O, Al, Mg and Co coexist (red outline). These regions correspond to Mg−Al composite hydroxides and Mg−Co−Al composite hydroxides ($Mg_xCo_{1-x}Al_y(OH)_z·nH_2O$), indicating that Co^{2+} can also replace Al^{3+} to form composite hydroxides.

The analysis above suggests that the presence of Al^{3+} causes a significant decrease in the pH at which Ni^{2+} and Co^{2+} initiate and complete precipitation, resulting in their co-precipitation loss during Al and Sc enrichment. The primary loss pathway is the formation of composite hydroxides. Additionally, a high Mg concentration can further decrease the pH at which Ni^{2+} and Co^{2+} initiate and complete precipitation, thereby promoting the formation of composite hydroxides.

3.5 Titration curves of different nitrate solutions

The pH titration curve can intuitively show the change in the pH of a solution as acid or alkali is added, thereby allowing the determination of the hydrolysis behavior of metal ions [32]. To further confirm the formation of composite hydroxides

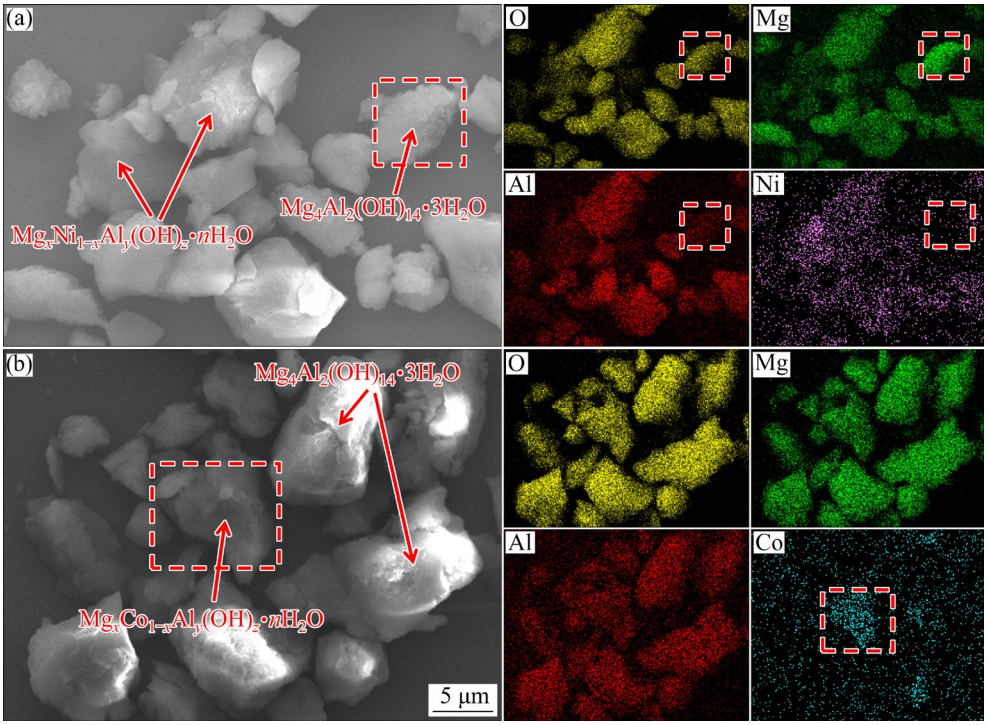

Fig. 11 SEM−EDS analysis of precipitates for mixed $Al(NO_3)_3$, $Ni(NO_3)_2$ and $Mg(NO_3)_2$ (a), and $Al(NO_3)_3$, $Co(NO_3)_2$ and $Mg(NO_3)_2$ (b) solutions

involving Al^{3+} and $Ni^{2+}/Co^{2+}/Mg^{2+}$, the pH titration curves of different nitrate solutions were measured. First, the forward and reverse titration curves for the $Al(NO_3)_3$ solution are presented in Fig. 12(a). The solution pH change can be mainly divided into three stages. In the first stage, with the addition of KOH, the solution pH gradually increases, but the pH has not yet reached the precipitation point of Al^{3+}. In the second stage, white colloidal precipitates start to appear when the pH reaches around 4.0, and the increase in solution pH slows down. During this stage, the added KOH primarily reacts with Al^{3+} to form $Al(OH)_3$. In the third stage, as Al^{3+} is completely hydrolyzed, the solution pH rises sharply, further addition of KOH significantly increases the pH. The reverse titration curve, obtained by adding HNO_3, indicates that the trend in the solution pH change is consistent with that observed during the forward titration. The pH initially drops sharply, stabilizes, and then gradually decreases. These results suggest that precipitation and dissolution are reversible processes, demonstrating that Al^{3+} undergoes a cyclical transformation from Al^{3+} to $Al(OH)_3$ and back to Al^{3+}.

Subsequently, the titration curves of the single-component $Ni(NO_3)_2$ solution and the mixed $Al(NO_3)_3$ and $Ni(NO_3)_2$ solution were also plotted in Fig. 12(b). In the single-component $Ni(NO_3)_2$ solution, with the addition of KOH, the solution pH initially rises, stabilizes for a while, and then increases again. This stable pH phase (around pH 7.8) primarily reflects the extensive hydrolysis of Ni^{2+}. Furthermore, notable differences are observed in the pH titration curves between the mixed $Al(NO_3)_3$ and $Ni(NO_3)_2$ solution and the sole $Ni(NO_3)_2$ solution. Initially, pH remains stable at around 4.0, due to the Al^{3+} hydrolysis. Interestingly, once the volume of added KOH roughly surpasses

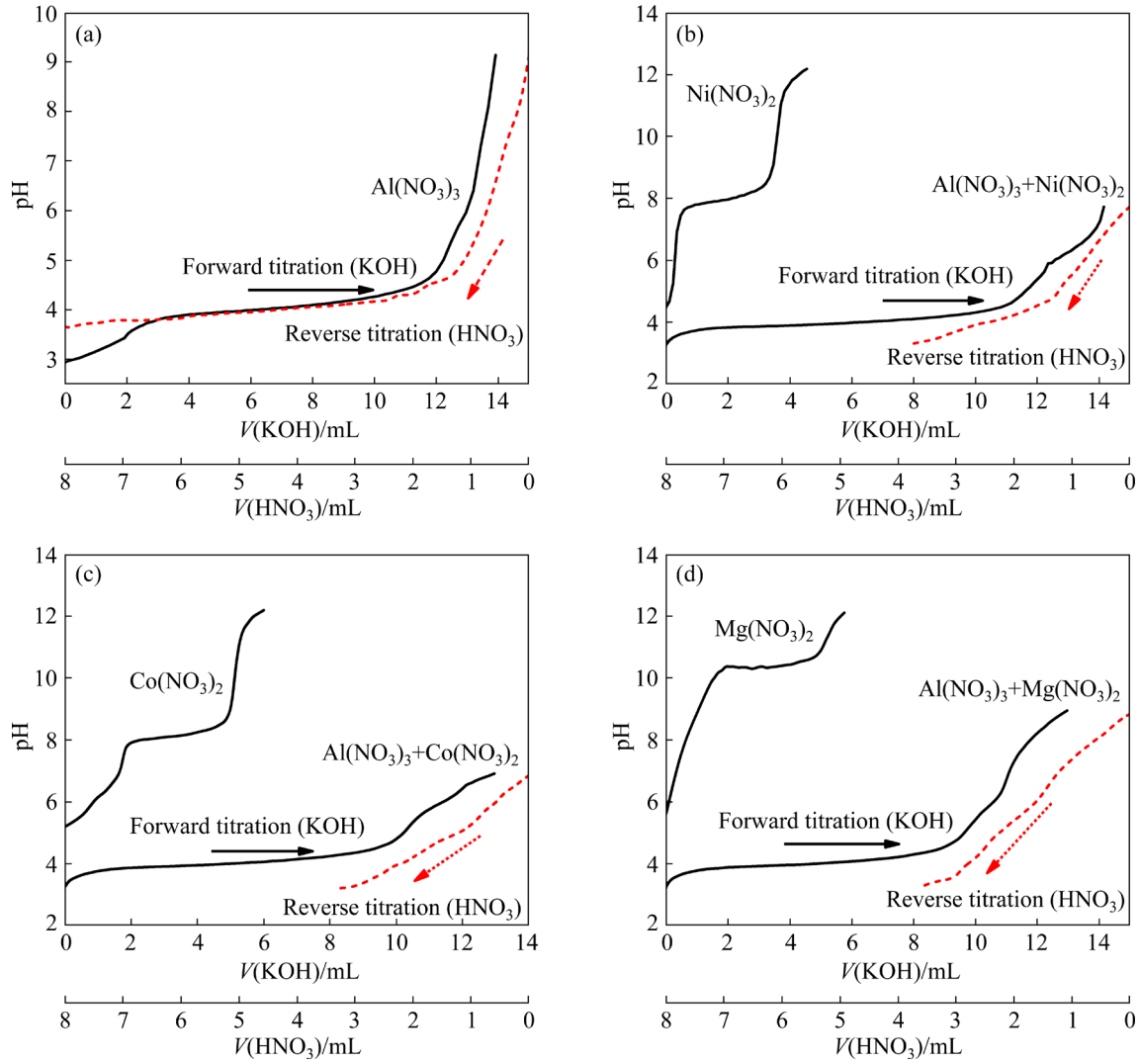

Fig. 12 pH titration curves of different nitrate solutions

11.0 mL, the solution pH shows only a slow rise. Theoretically, if Al^{3+} and Ni^{2+} precipitate sequentially, the complete hydrolysis of Al^{3+} should sharply elevate the solution pH to the point where Ni^{2+} begins to hydrolyze (approximately 7.80). However, the hypothetical sharp increase is absent in Fig. 12(b). Instead, the solution pH rises slowly following Al^{3+} hydrolysis, indicating that Ni^{2+} gradually precipitates. Compared with the single-component $Ni(NO_3)_2$ solution, the Ni^{2+} precipitation pH significantly decreases, indicating that Ni^{2+} does not solely generate $Ni(OH)_2$ in the mixed $Al(NO_3)_3$ and $Ni(NO_3)_2$ solution but instead forms composite hydroxides with the produced $Al(OH)_3$. In addition, if the precipitation of Al^{3+} and Ni^{2+} solely involved their hydrolysis to form respective hydroxides, the forward and reverse titration curves would exhibit similar trends. However, the reverse titration process significantly diverges from the forward process. Consequently, it can be inferred that during hydrolysis, Ni−Al composite hydroxide are formed. The dissolution and formation processes of composite hydroxide are irreversible, giving rise to the observed differences between the forward and reverse titration processes.

Then, the titration curves of single-component $Co(NO_3)_2$ and $Mg(NO_3)_2$ solutions, as well as those of the mixed solutions of $Al(NO_3)_3$ and $Co(NO_3)_2$, and $Al(NO_3)_3$ and $Mg(NO_3)_2$, were analyzed. The pH at which Co^{2+} begins to precipitate in the single-component $Co(NO_3)_2$ solution is around 8.0, and this value decreases significantly in the mixed nitrate solution (Fig. 12(c)). Moreover, the changing trend of the forward and reverse titration curves has an obvious difference, similar to that observed in the mixed $Al(NO_3)_3$ and $Ni(NO_3)_2$ solution. The results suggest that Al^{3+} and Co^{2+} can also form the Co−Al composite hydroxide. Similarly, the pH at which Mg^{2+} begins to precipitate in the single-component $Mg(NO_3)_2$ solution is close to 10.0, and this value decreases in the mixed $Al(NO_3)_3$ and $Mg(NO_3)_2$ solution (Fig. 12(d)). The discrepancy between the forward and reverse titration curves further substantiates the formation of Mg−Al composite hydroxide.

The above analysis indicates that composite hydroxides can form between Al and Ni, Co, or Mg in mixed nitrate solutions. Because Al^{3+} has a higher charge and a smaller radius than Ni^{2+}, Co^{2+} and Mg^{2+}, it has a strong ability to bind oxygen. This can weaken the O—H covalent bond in $Al(OH)_3$, and the shared electron pairs are attracted towards O, resulting in $Al(OH)_3$ exhibiting a certain degree of acidity. When Ni^{2+}, Co^{2+} and Mg^{2+} are present, they can react with $Al(OH)_3$ to form the Al^{3+}—O—Me^{2+}—OH bond (Me^{2+} represents Ni^{2+}, Co^{2+}, or Mg^{2+}). In addition, the difficulty of forming composite hydroxide between $Al(OH)_3$ and Me^{2+} is related to the alkalinity of $Me(OH)_2$. The stronger the alkalinity of $Me(OH)_2$ is, the easier it is to form composite hydroxides. Therefore, it can be concluded that the formation trend is Mg−Al > Co−Al > Ni−Al.

Generally speaking, the acidity of composite hydroxides is stronger than that of simple metal hydroxides, and the generated composite hydroxides are difficult to react with the acids at the pH corresponding to the forward titration process. Therefore, the forward and reverse titration curves exhibit remarkable differences in the mixed nitrate solutions. Moreover, the greater the difference between the forward and reverse titration curves is, the more stable the formed composite hydroxide will be. Hence, the stability of composite hydroxides follows this order: Mg−Al > Co−Al > Ni−Al. Combining the above analyses, the formation process of composite hydroxides is depicted in Fig. 13.

In summary, adsorption and co-precipitation are the main loss pathways of Ni and Co during Al and Sc enrichment. The adsorption loss is attributed to the Al−Sc precipitate, while co-precipitation loss is due to the formation of composite hydroxides. Ni and Co that are lost due to adsorption can be recovered through washing. The co-precipitation loss is closely related to the neutralizing agent. MgO particles will hydrate to form $Mg(OH)_2$ on their surfaces. $Mg(OH)_2$ has high alkalinity and low solubility, leading to high alkalinity in some areas of the liquid phase. This, in turn, provides conditions for the formation of composite hydroxides. In future work, various strategies such as reducing the concentration of magnesium oxide, increasing the stirring speed, and altering the precipitation methods can be considered to minimize the formation of locally alkaline regions, thereby reducing the co-precipitation loss of Ni and Co.

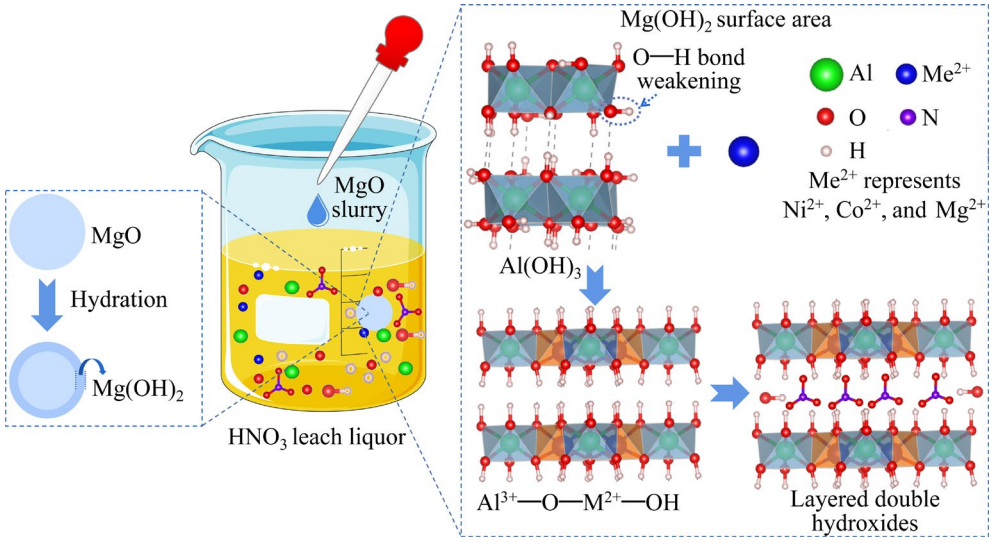

Fig. 13 Schematic diagram for formation of composite hydroxides

4 Conclusions

(1) Selective enrichment of Al and Sc cannot be achieved through MgO neutralization precipitation. At pH 4.5 and 50 °C, while 99.32% of Al and 99.18% of Sc can be enriched, a significant loss of 43.2% Ni and 40.3% Co also occurs under these conditions.

(2) The adsorption of Al−Sc precipitate is one of the important loss pathways for Ni and Co. Adsorption rates of Ni^{2+} and Co^{2+} are 9.35% and 12.50%, respectively, under the optimal conditions for enriching Al and Sc. In addition, Ni^{2+} and Co^{2+} do not hydrolyze to form their respective hydroxides during enrichment, which is not the pathway for their loss.

(3) During the process of hydrolysis, Al^{3+} forms not only $Al(OH)_3$ but also Mg−Al composite hydroxides. Furthermore, precipitated $Al(OH)_3$ can combine with Ni^{2+}, Co^{2+} and Mg^{2+} in mixed nitrate solutions, yielding composite hydroxides such as Ni−Al, Co−Al, Mg−Al, and Ni/Co−Mg−Al. An elevated Mg concentration enhances the formation of these composite hydroxides, significantly lowering the precipitation pH range for Ni^{2+}, Co^{2+} and Mg^{2+}, thereby contributing to co-precipitation loss.

(4) $Al(OH)_3$ tends to exhibit acidity in the alkaline region that allows its O—H bond to be easily broken, providing prerequisites for the formation of Me−Al composite hydroxides. Me^{2+} can react with $Al(OH)_3$ to form the Al^{3+}—O—Me^{2+}—OH bond. Titration curves of different nitrate solutions further demonstrate the formation of composite hydroxides and also confirm that the formation trend is Mg−Al > Co−Al > Ni−Al.

CRediT authorship contribution statement

Jian-cheng YU: Conceptualization, Writing − Original draft, Writing − Review & editing; **Bao-zhong MA:** Writing − Review & editing, Supervision, Project administration; **Long-fei SHI:** Resources, Validation; **Zhi-he CAO:** Validation, Visualization; **Yu-bo LIU:** Methodology; **Cheng-yan WANG:** Supervision, Project administration, Funding acquisition.

Declaration of competing interest

The authors declare that they have no known competing financial interests or personal relationships that could have appeared to influence the work reported in this paper.

Acknowledgments

This work was supported by the National Natural Science Foundation of China (No. U2202254).

References

[1] MESHRAM P, ABHILASH, PANDEY B D. Advanced review on extraction of nickel from primary and secondary sources [J]. Mineral Processing and Extractive Metallurgy Review, 2019, 40: 157−193.

[2] KAYA Ş, DITTRICH C, STOPIC S, FRIEDRICH B. Concentration and separation of scandium from Ni laterite ore processing streams [J]. Metals, 2017, 7: 557−563.

[3] SUN Yuan-wei, WANG Zi-yi, ZHAO Xiang-jin, LIU Zhong-li, CAO Fu-hua. Effects of Sc addition on

microstructure, phase evolution and mechanical properties of $Al_{0.2}$CoCrFeNi high-entropy alloys [J]. Transactions of Nonferrous Metals Society of China, 2023, 33: 3756−3769.

[4] OXLEY A, BARCZA N. Hydro-pyro integration in the processing of nickel laterites [J]. Minerals Engineering, 2013, 54: 2−13.

[5] XIAO Jun-hui, XIONG Wen-liang, ZOU Kai, CHEN Tao, LI Hong, WANG Zhen. Extraction of nickel from magnesia-nickel silicate ore [J]. Journal of Sustainable Metallurgy, 2021, 7: 642−652.

[6] PANDEY N, TRIPATHY S K, PATRA S K, JHA G. Recent progress in hydrometallurgical processing of nickel lateritic ore [J]. Transactions of the Indian Institute of Metals, 2023, 76: 11−30.

[7] GUO Qiang, QU Jing-kui, HAN Bing-bing, WEI Guang-ye, ZHANG Pei-yu, QI Tao. Dechromization and dealumination kinetics in process of Na_2CO_3-roasting pretreatment of laterite ores [J]. Transactions of Nonferrous Metals Society of China, 2014, 24: 3979−3986.

[8] MA Dong-lai, ZHAO Jian-bo, HU Qing-qing, LU Xue-ming, YOU Yang, YOU Zhi-xiong, LÜ Xue-wei. Effect of additives on growth of ferronickel grains and metal−slag separation behavior [J]. Transactions of Nonferrous Metals Society of China, 2022, 32: 3459−3468.

[9] YU Yang, LI Bao-kuan, FANG Zheng-zhe, WANG Chang-jun. Energy and exergy analyses of pellet smelting systems of cleaner ferrochrome alloy with multi-energy supply [J]. Journal of Cleaner Production, 2021, 285: 124893−124905.

[10] CHEN Yong-qiang, ZHAO Hong-liang, WANG Cheng-yan. Two-stage reduction for the preparation of ferronickel alloy from nickel laterite ore with low Co and high MgO contents [J]. International Journal of Minerals Metallurgy and Materials, 2017, 24: 512−522.

[11] YU Jin-cheng, QIAN Jue-shi, WANG Fan, QIN Ji-hui, DAI Xiao-bing, YOU Chao, JIA Xing-wen. Study of using dolomite ores as raw materials to produce magnesium phosphate cement [J]. Construction and Building Materials, 2020, 253: 119147−119159.

[12] ZHAI Yu-chun, MU Wen-ning, LIU Yan, XU Qian. A green process for recovering nickel from nickeliferous laterite ores [J]. Transactions of Nonferrous Metals Society of China, 2010, 20: s65−s70.

[13] KURSUNOGLU S, KAYA M. Atmospheric pressure acid leaching of Caldag lateritic nickel ore [J]. International Journal of Mineral Processing, 2016, 150: 1−8.

[14] MACCARTHY J, NOSRATI A, SKINNER W, ADDAI-MENSAH J. Atmospheric acid leaching mechanisms and kinetics and rheological studies of a low grade saprolitic nickel laterite ore [J]. Hydrometallurgy, 2016, 160: 26−37.

[15] GUO Xue-yi, SHI Wen-tang, LI Dong, TIAN Qing-hua. Leaching behavior of metals from limonitic laterite ore by high pressure acid leaching [J]. Transactions of Nonferrous Metals Society of China, 2011, 21: 191−195.

[16] SHEN Xiao-yi, HUANG Yan-xiang, SHAO Hong-mei, WANG Yuan, HAN Qing, CHEN Jian-she, LI Bin-chuan, ZHAI Yu-chun. Facile fabrication of spherical flower-like $Mg(OH)_2$ and its fast and efficient removal for heavy metal ions [J]. Transactions of Nonferrous Metals Society of China, 2022, 32: 3149−3162.

[17] IBRAHIM M H, BATSTONE D, VAUGHAN J, STEEL K. Electrochemical separation of sulfuric acid from magnesium sulfate solutions: Application for nickel laterite processing [J]. Separation and Purification Technology, 2024, 336: 126291−126300.

[18] LI Guang-hui, CHNE Yan-hu, MANG Chang-ye, TENG Xin, LUO Jun, RAO Ming-jun. Rao, Near-zero-waste approach for the treatment of saprolitic nickel laterite via a combined hydrometallurgical process [J]. ACS Sustainable Chemistry & Engineering, 2023, 11: 6856−6865.

[19] OUSTADAKIS P, AGATZINI-LEONARDOU S, TSAKIRIDIS P E. Nickel and cobalt precipitation from sulphate leach liquor using MgO pulp as neutralizing agent [J]. Minerals Engineering, 2006, 19: 1204−1211.

[20] ZHOU Zheng-en, MA Bao-zhong, WANG Cheng-yan, CHEN Yong-qiang, ZHANG Wen-juan, HUANG Kun, Enrichment of scandium and aluminum from limonitic laterite during the nitric acid pressure leaching process [J]. Hydrometallurgy, 2022, 208: 105819−105829.

[21] FARIS N, WHITE J, MAGAZOWSKI F, FISCHMANN A J, JONES L A, TARDIO J, MADAPUSI S, GROCOTT S, BHARGAVA S K. An investigation into potential pathways for nickel and cobalt loss during impurity removal from synthetic nickel laterite pressure acid leach solutions via partial neutralisation [J]. Hydrometallurgy, 2021, 202: 105595−105607.

[22] ZHOU Zheng-en, MA Bao-zhong, WANG Cheng-yan, CHEN Yong-qiang, WANG Ling. Recovery of scandium and aluminum from limonitic laterite intermediate product [J]. Minerals Engineering, 2022, 188: 107844−107855.

[23] ZHAO Ding, MA Bao-zhong, WANG Cheng-yan, ZHANG Yu-qing, SHI Shu-yang, CHEN Yong-qiang. Investigation of the thermal behavior of $Mg(NO_3)_2·6H_2O$ and its application for the regeneration of HNO_3 and MgO [J]. Chemical Engineering Journal, 2022, 433: 133804−133815.

[24] MCDONALD R G, WHITTINGTON B I. Atmospheric acid leaching of nickel laterites review. Part I: Sulphuric acid technologies [J]. Hydrometallurgy, 2008, 91: 35−55.

[25] da SILVA M D F, DE SOUSA OLIVEIRA M R, DOS SANTOS I D, RADINO-ROUSE P, MANSUR M B. Iron precipitation strategies from nickel laterite ore sulfuric acid leach liquor [J]. Mineral Processing and Extractive Metallurgy Review, 2022, 43: 28−39.

[26] MANG Chang-ye, LI Guang-hui, CHEN Yan-hu, LUO Jun, RAO Ming-jun, JIANG Tao. Efficient removal of iron during partial neutralization of nickel laterite acid leach solution: DFT calculation and experimental verification of mechanism [J]. Hydrometallurgy, 2023, 220: 106090−106100.

[27] MILLER A, WILDEMAN T, FIGUEROA L. Zinc and nickel removal in limestone based treatment of acid mine drainage: The relative role of adsorption and co-precipitation [J]. Applied Geochemistry, 2013, 37: 57−63.

[28] BHATT P, CHATTOPADHYAY S, MISRA K P, MADAN D, HALDER N. Effect of temporal pH variation of the reaction mixture on $Mg(OH)_2$ morphology precipitated from an aqueous $Mg(NO_3)_2$−NaOH system [J]. Advanced Powder Technology, 2021, 32: 2289−2299.

[29] INTASA-ARD S, OGAWA M. Simple and cost-effective

mass production of nitrate type MgAl layered double hydroxide: Titration from concentrated solution [J]. Applied Clay Science, 2022, 228: 106615−106622.

[30] DUAN Meng-ting, LIU Shan-jing, JIANG Qi-ming, GUO Xing-mei, ZHANG Jun-hao, XIONG Sheng-lin. Recent progress on preparation and applications of layered double hydroxides [J]. Chinese Chemical Letters, 2022, 33: 4428−4436.

[31] PAIKARAY S, ESSILFIE-DUGHAN J, HENDRY M J. Ionic substitution of Mg^{2+} for Al^{3+} and Fe^{3+} with octahedral coordination in hydroxides facilitate precipitation of layered double hydroxides [J]. Geochimica et Cosmochimica Acta, 2018, 220: 217−234.

[32] EGGERMONT S G F, PRATO R, DOMINGUEZ-BENETTON X, FRANSAER J. Metal removal from aqueous solutions: Insights from modeling precipitation titration curves [J]. Journal of Environmental Chemical Engineering, 2020, 8: 103596−103603.

腐殖型红土矿硝酸浸出液富集 Al 和 Sc 时 Ni 与 Co 的损失行为

郁建成[1,2]，马保中[1,2]，石龙飞[1,2]，曹志河[1,2]，刘玉博[1,2]，王成彦[1,2]

1. 北京科技大学 绿色低碳钢铁冶金全国重点实验室，北京 100083；
2. 北京科技大学 冶金与生态工程学院，北京 100083

摘　要：分析了腐殖型红土矿硝酸浸出液在富集 Al 和 Sc 过程中 Ni 和 Co 的损失途径。尽管超过 99%的 Al 和 Sc 可以被富集，但约 40%的 Ni 和 Co 也会损失。Al−Sc 沉淀的吸附是造成 Ni 和 Co 损失的重要原因。随后，对不同硝酸盐溶液中金属离子的沉淀行为进行研究。结果表明：Ni^{2+}和 Co^{2+}不会水解形成各自的氢氧化物。Ni^{2+}、Co^{2+}和 Mg^{2+}可与 $Al(OH)_3$ 沉淀形成复合氢氧化物，降低 Ni^{2+}和 Co^{2+}开始沉淀的 pH 值，导致它们共沉淀损失。高浓度 Mg^{2+}可促进这些复合氢氧化物的形成。最后，测定了不同硝酸盐体系的滴定曲线，进一步证实了 Me−Al 复合氢氧化物的形成，其形成趋势为 Mg−Al＞Co−Al＞Ni−Al。

关键词：红土矿；硝酸浸出液；金属损失；水解沉淀；复合氢氧化物

(Edited by Xiang-qun LI)